View metadata, citation and similar papers at core.ac.uk

brought to you by CORE

provided by HAL-CEA

Mutations in TUBG1, DYNC1H1, KIF5C and KIF2A cause malformations of cortical development and microcephaly.

Karine Poirier, Nicolas Lebrun, Loic Broix, Guoling Tian, Yoann Saillour, Cécile Boscheron, Elena Parrini, Stephanie Valence, Benjamin Saint Pierre, Madison Oger, et al.

To cite this version:

Karine Poirier, Nicolas Lebrun, Loic Broix, Guoling Tian, Yoann Saillour, et al.. Mutations in TUBG1, DYNC1H1, KIF5C and KIF2A cause malformations of cortical development and microcephaly.. Nature Genetics, Nature Publishing Group, 2013, 45 (6), pp.639-47. <10.1038/ng.2613>. <inserm-00838073>

HAL Id: inserm-00838073

http://www.hal.inserm.fr/inserm-00838073

Submitted on 8 Oct 2013

HAL is a multi-disciplinary open access archive for the deposit and dissemination of scientific research documents, whether they are published or not. The documents may come from teaching and research institutions in France or abroad, or from public or private research centers.

L'archive ouverte pluridisciplinaire **HAL**, est destinée au dépôt et à la diffusion de documents scientifiques de niveau recherche, publiés ou non, émanant des établissements d'enseignement et de recherche français ou étrangers, des laboratoires publics ou privés.

Mutations in TUBG1, DYNC1H1, KIF5C and KIF2A cause malformations of cortical development and microcephaly

Karine Poirier[1,2], Nicolas Lebrun[1,2], Loic Broix[1,2*], Guoling Tian[3*], Yoann Saillour[1,2], Cécile Boscheron[4], Elena Parrini[5,6], Stephanie Valence[1,2], Benjamin SaintPierre[1,2], Madison Oger[1,2], Didier Lacombe[7], David Geneviève[8], Elena Fontana[9], Franscesca Darra[9], Claude Cances[10], Magalie Barth[11,12], Dominique Bonneau[11,12], Bernardo Dalla Bernadina[9], Sylvie N'Guyen[13], Cyril Gitiaux[1,2,14,], Philippe Parent[15], Vincent des Portes[16], Jean Michel Pedespan[17], Victoire Legrez[18], Laetitia Castelnau-Ptakine[1,2], Patrick Nitschke[19], Thierry Hieu[19], Cecile Masson[19], Diana Zelenika[20], Annie Andrieux[4], Fiona Francis[21,22], Renzo Guerrini[5,6], Nicholas J. Cowan[3], Nadia Bahi-Buisson[1,2,14**], Jamel Chelly[1,2**]

1. Institut Cochin, Université Paris-Descartes, CNRS (UMR 8104), Paris, France,
2. Inserm, U1016, Paris, France,
3. Department of Biochemistry and Molecular Pharmacology, New York University Medical Center, New York, NY 10016
4. Institut des Neurosciences, Inserm, U836, Université Joseph Fourier – Grenoble 1, France
5. Pediatric Neurology Unit and Laboratories, Children's Hospital A. Meyer-University of Florence, Italy,
6. IRCCS Stella Maris Foundation. Pisa, Italy
7. Department of Medical Genetics, CHU Pellegrin, Bordeaux, France,
8. Department of Medical Genetics, Université Montpellier 1, INSERM U844, 34000 Montpellier, France,
9. UOC di Neuropsichiatria Infantile, Azienda Ospedaliera Univesritaria di Verona, Italy,
10. Département de Pédiatrie, CHU Toulouse, France,
11. INSERM: U694, Université d'Angers, CHU 4, Rue Larrey 49033 Angers Cedex, France,
12. Service de génétique CHU Angers, Angers, France,
13. Clinique Médicale Pédiatrique, CHU de Nantes, Nantes, France,
14. Unité de Neurologie Pédiatrique, Hôpital Necker Enfants Malades, Université Paris Descartes, France,
15. Service de Pédiatrie et Génétique Médicale
, Brest, France,
16. Centre de référence déficiences intellectuelles de causes rares, CHU Lyon, Université Lyon1, L2C2 CNRS, Bron , France
17. Service de Pédiatrie, CHU Pellegrin, Bordeaux, France,
18. CHU Bicetre Service Neuropediatrie, Le Kremlin Bicetre, France
19. Bioinformatics plateform, Université Paris Descartes, Paris, France,
20. Centre National de Génotypage (CNG), Evry, France,
21. INSERM - Institut du Fer à Moulin, Paris, F75005, France,
22. Université Pierre et Marie Curie, Paris F75005, France,

[*] and [**] Equal contribution

Corresponding authors
Jamel Chelly
Institut Cochin –
Genetics and pathophysiology of neurodevelopmental disorders
CHU Cochin, 24 Rue du Faubourg Saint Jacques
75014 Paris
33 1 44 41 24 10
jamel.chelly@inserm.fr

Nicholas J. Cowan
Department of Biochemistry and Molecular Pharmacology
New York University Langone Medical Center
550 First Avenue
New York NY 10016. USA
Nicholas.Cowan@nyumc.org

Abstract

The genetic causes of malformations of cortical development (MCD) remain largely unknown. Here we report the discovery of multiple disease-causing missense mutations in *TUBG1, DYNC1H1* and *KIF2A*, as well as a single germline mosaic mutation in *KIF5C*. We find a frequent recurrence of mutations in *DYNC1H1*, implying that this gene is a major locus implicated in unexplained MCD. The mutations in *KIF5C, KIF2A* and *DYNC1H1* drastically affect ATP hydrolysis, productive protein folding or microtubule binding, while suppression of *Tubg1* expression *in vivo* interferes with proper neuronal migration and expression of *Tubg1* mutations in *S. cerevisiae* results in disruption of normal microtubule behaviour. Our data reinforce the importance of centrosome- and microtubule-related proteins in cortical development and strongly suggest that microtubule-dependent mitotic and post-mitotic processes are major contributors to the pathogenesis of MCD.

Introduction

The formation of the complex architecture of the mammalian brain requires coordinated timing of proliferation, migration and layering, as well as differentiation of distinct neuronal populations[1,2]. Significant insights into these developmental processes have emerged through genetic and neurobiological investigations of the mechanisms underlying disorders of cortical development. These disorders include lissencephaly/pachygyria (LIS), polymicrogyria (PMG) and microcephaly[3-7]. Many are associated with severe intellectual disability and epilepsy, and have traditionally been classified based on which biological process (proliferation, migration and cortical organization) is likely to be affected[5].

Genetic studies in humans and mice have identified a spectrum of mutations in genes involved in an array of crucial processes that often disrupt the development of the cerebral cortex and can lead to severe cortical malformations. Aside from genes such as ARX and WDR62 (reviewed in[5]), the predominant importance of genes encoding cytoskeletal proteins has become evident. For example, mutations in *DCX* and *LIS1*, both of which encode proteins involved in microtubule homeostasis, are associated with a large spectrum of neuronal migration disorders (reviewed in[3]). More recently, new syndromes have been described that are associated with mutations in α- or β-tubulin encoding genes such as *TUBA1A, TUBB2B*, *TUBB3* and *TUBB5*. These tubulin-related cortical dysgeneses are thought to involve a combination of abnormal neuronal proliferation, migration, differentiation and axonal guidance[8-10]. The vanishing boundaries between disorders of neuronal migration, cortical organization and proliferation have been highlighted by the recent identification of mutations in *WDR62* and its implication in a large spectrum of malformations that includes pachygyria, lissencephaly, PMG, schizencephaly, hippocampal and cerebellar abnormalities[11,12]. These findings, together with genetic and functional data, support the hypothesis that MCD-related genes are involved at multiple developmental stages, and that proliferation and migration are genetically and functionally interdependent.

Sporadic unexplained cases of MCD are by far the most common, and identification of causative mutations remains a challenging task, not least because many result from *de novo* mutations (reviewed in[13]). To extend the spectrum of genes involved in MCD, we used an exome sequencing approach and focused on variations in candidate genes encoding centrosomal and microtubule-related proteins.

Results

Subgroups of patients with MCD analysed by whole exome sequencing

We selected 16 patients with either lissencephaly/pachygyria (6 patients) or polymicrogyria (10 patients) associated with one of the following features: microcephaly (head circumferences more than 2-3 SD below the mean for age), dysgenesis of the cerebellum, brainstem or basal ganglia or agenesis/dysgenesis of the corpus callosum (Supplementary Table 1). Supplementary Figure 1 highlights the overall experimental workflow for detecting and prioritizing sequence variants and validation of the MCD-related genes detailed below. All families had a single affected member (sporadic cases), except one in which MCD was diagnosed in four individuals (P20, Fig. 1a). For all patients, mutations in known MCD genes (*LIS1, DCX, TUBA1A, TUBB2B, TUBB3* and *GPR56*) and pathogenic CNVs had been previously excluded.

We applied whole-exome sequencing methodology and, in line with previous studies[14,15], identified around 21,500 variations affecting essential splicing site and coding regions for each patient. After application of variant filtering using available genomic databases (dbSNP, 1k genome, EVS and a local Paris Descartes Bioinformatics platform database) and exclusion of all variants found with a frequency greater than 1%, an average of 390 variants per patient was identified (Supplementary Table 2).

A KIF5C germline mosaic mutation

At first glance, in family P20 (Fig. 1a) containing 4 affected boys with severe MCD and microcephaly, the apparent transmission of the recurrent phenotype through the mother suggests the segregation in this family of an X-linked disorder. However, we found no linkage between the disease and a large set of X-linked markers (Supplementary Fig. 2a and 2b). Exclusion of the X chromosome and the unlikely autosomal recessive inheritance of the disorder (because of its occurrence even when the progenitor father was different) led us to consider a mosaic germline mutation in the mother. We therefore performed whole exome sequencing (using DNA from patient III-1, Fig. 1a) and genome-wide SNP genotyping using high-density microarray (see Materials and Methods) of affected members and their mother to identify shared segments transmitted by the

mother (Supplementary Table 3). Among the shared genomic regions, we found a region of 44 Mb on chromosome 2 (Supplementary Fig. 2c and 2d) which harbours a missense variant (c.710A>T, p.E237V) in the kinesin 5C gene (*KIF5C*) (Table 1). We tested the segregation of this variation in the family and found it to be present in all affected individuals, but absent in the mother's DNA (derived from blood) and in the healthy son (Fig. 2b; see also Supplementary Fig. 2d and 2e). Also, in the case of the foetus corresponding to the most recent medical abortion, expression of KIF5C alleles was tested by RT-PCR using total RNA extracted from brain and lung; we found that both alleles were expressed to the same extent (see Supplementary Fig. 3a). Taken together, these data are consistent with a *KIF5C* germline mosaic mutation as the likely cause of the disease phenotype in the P20 family.

KIF5C encodes a member of the kinesin superfamily of proteins, most of which are ATP-dependent molecular motors involved in intracellular transport along microtubules[16]. The p.E237V mutation is located in the microtubule-interacting domain (Fig 1b), and 3D modelling shows a surface location of this residue within the motor domain (Fig. 1c). The mutation might be expected to affect conformational changes of the switch II loop, which is required for microtubule-dependent activation of the motor[16].

To assess the consequences of the mutation on KIF5C function, we expressed and purified the motor domains of both wild type and mutant as recombinant proteins in E. coli (Supplementary Fig. 3b). The mutant protein behaved as a native species upon gel filtration (Supplementary Fig. 3c), eliminating the possibility that the mutation might result in a completely misfolded or aggregated protein. We first compared the ability of the wild type and mutant proteins to bind to microtubules, and found no significant difference (Fig. 1d). However, when we measured the ability of each KIF to hydrolyse ATP in a microtubule-dependent assay, we found a complete absence of measurable hydrolysis in the case of the mutant protein (Fig. 1e). This finding is consistent with the location of the mutated residue in the crystal structure, as well as with the deleterious effect of the mutation in the severe MCD diagnosed in P20 family (Supplementary Fig. 3d).

The consequences of the p.E237V mutation were also tested *in vivo*. We expressed wild type and mutant KIF5C proteins by transfection in COS-7 cells, and compared their distribution and localization by double

label immunofluorescence. As previously reported[17], we found a diffuse cytoplasmic distribution of wild type KIF5C with an enrichment, as fluorescent puncta, along microtubules and in cortical regions of the cell (Fig. 1f and Supplementary Fig. 3e). In contrast, we found that mutant KIF5C heavily co-localises with and decorates microtubules throughout the cell, but does not appear as puncta or accumulate in cortical clusters (Fig. 1f and Supplementary Fig. 3e). This result is consistent with the loss of ATPase activity shown by the in vitro assay and is also in agreement with earlier work concerning a non-motile mutant Kif5c (p.T93N) that binds to microtubules but inhibits ATP hydrolysis[18]. In the case of the mutation identified in this family, both KIF5C alleles are expressed. In common with most kinesins, KIF5C functions as a tetramer consisting of two heavy chains and two light chains. It is therefore possible that the mutant KIF5C could titrate out the wild type isoform and act via a dominant negative effect.

Mutations in KIF2A

The identification of a *KIF5C* mutation prompted us to screen this gene in a cohort of 162 patients affected by various MCD (see Material and Methods), and analyse all other variations in kinesin genes revealed by WES and not reported in databases. Among 15 heterozygous variations, we found a single *de novo* missense change in *KIF2A* (c.961C>G, p.H321D) in a female patient (P462, Table 1) with frontal band heterotopia and posterior predominant pachygyria, severe congenital microcephaly and neonatal onset seizures (Fig. 2a and 2b, Table 1, Supplementary Table 1 and Supplementary Table 4). We subsequently screened the *KIF2A* gene (coding exons and their flanking sequences) in the same cohort of patients and identified a second *de nov*o *KIF2A* missense variation, c.950G>A, p.S317N (P147: Table 1 and Fig. 2a and 2b) in a girl affected by congenital microcephaly and posterior predominant agyria/pachygyria (Fig. 2a and Supplementary table 4).

KIF2A is a member of the M-kinesins (kinesin-13 family) in which the motor domain is located in the middle of the protein (Fig. 2b). Rather than a direct involvement in microtubule-based motility, KIF2A functions by driving the ATP-dependent depolymerization of microtubules[19]. In addition to a potential deleterious effect predicted by PolyPhen-2 and SIFT algorithms[20,21] (Supplementary Table 5), inspection of the protein structure (PDB 2GRY, Fig. 2c) shows that both conserved residues p.S317 and p.H321 are located around the nucleotide binding pocket, suggesting that the ability of KIF2A mutants to bind and/or hydrolyse ATP is

likely to be impaired. To investigate this possibility, we expressed the wild type and mutant ATP binding domains (amino acids 126 – 526) in E. coli as recombinant C-terminally His_6-tagged proteins. We found that the wild type protein was present as a conspicuous Coomassie-stained band in soluble extracts of host cells (Fig. 2d, panel 1, lane 1, arrowed). However, the two mutant proteins expressed in parallel soluble extracts were not convincingly identifiable (Fig. 2d, panel 1, lanes 2 and 3); indeed, upon affinity purification, the mutant KIF2A proteins were recovered at a very substantially reduced level compared to the wild type control (Fig. 2d, panel 4 and corresponding Western blot), appearing instead at a higher level (relative to the wild type control) in the insoluble fraction following host cell lysis (Fig. 2d, panel 2). These data imply that the mutations lead to substantially reduced solubility as a result of misfolding, and therefore at a minimum result in a reduced yield of functional protein. We also transfected constructs engineered for the expression of these KIF2A mutations into COS-7 and human fibroblast cells, and analysed them by immunofluorescence. We consistently found that both overexpressed mutant KIF2A proteins (p.H321D and p.S317N) had an abnormal cellular localization (Fig. 2e and Supplementary Fig. 4a). We also examined endogenous mutant KIF2A in fibroblasts derived from the patient bearing the c.961C>G, p.H321D mutation and found similar results (Fig. 2f).

In view of the fact that both KIF2A alleles are expressed in patient fibroblasts (Supplementary Fig. 4b) and that the KIF2A molecule functions as a dimer[22], our in vitro and in vivo data are consistent with a dominant-negative effect of these mutations.

Recurring mutations in *DYNC1H1* and *TUBG1*

We searched for the recurrence of mutations in the same gene in unrelated patients with similar phenotypes and identified two variations in *DYNC1H1* (P122 and P398, Table 1, Supplementary Table 4 and Fig. 3) and two others in *TUBG1* (P367 and P388, Table 1, Supplementary Table 4 and Fig. 4). The *de novo* mutations in *DYNC1H1* were found in patients with complex MCD from group A (PMG group, Supplementary Table 1), while those in *TUBG1* occurred in two patients with MCD from group B (agyria/pachygyria group, Supplementary Table 1). Because of the large spectrum of MCD associated with mutations in genes such as *TUBA1A*, *TUBB2B* and *WDR62*[11,12,23], we analysed all variations detected in these two genes in either group

and identified (and confirmed) one additional *de novo* variation in *DYNC1H1* in a patient from Group B (P217, Table 1 and Fig. 3a). To confirm the involvement of *DYNC1H1* and *TUBG1* in complex MCD, we screened *TUBG1* and DYNC1H1 coding exons in the cohort of 162 patients with MCD. Consistent with our exome sequencing findings, we identified a total of 6 additional *DYNC1H1* mutations (Table 1 and Supplementary Table 5). The finding of the same mutation (p.R3344Q) in two unrelated patients with a similar phenotype strongly supports the involvement of *DYNC1H1* in MCD. In the case of *TUBG1*, the screening revealed one additional mutation (P478, Table 1 and Fig. 4a). Whenever possible, analysis of parental DNAs demonstrated the *de novo* occurrence of these mutations, with the exception of *DYNC1H1* p.K3241T, which we identified as a familial form of MCD (Table 1, Supplementary Fig. 5). Consistent with a pathogenic effect, interspecies sequence comparison and prediction showed a high degree of conservation and potential deleterious effect of all residues involved (Supplementary Table 5).

***DYNC1H1* mutations**

Among the 11 patients (8 sporadic cases, and two brothers and their mother) reported here, re-examination of MRI sequences identified a wide range of brain malformations (Fig. 3b, Supplementary Table 4 and Discussion). Because mutations in *DYNC1H1* have been reported in families with dominant peripheral neuropathy and an axonal (type 2) form of Charcot Marie-Tooth disease (CMT2)[24,25], we re-evaluated our patients and found clear clinical evidence of peripheral neuropathy in 3 cases. This was further confirmed in one patient by nerve conduction studies.

DYNC1H1 (cytoplasmic dynein 1 heavy chain 1) protein is a large (>530 kDa) critical subunit of the cytoplasmic dynein complex[26,27]. The C-terminal region (AA 1846–4646) is the motor domain complex; it is arranged as a heptameric ring with 7 AAA domains and a stalk from which protrudes a microtubule-binding domain (BD)[26]. Interestingly, 6 out of the 8 mutations identified in patients with MCD are located in either the stalk domain, in AAA1 or in the linker region; the remaining two are in the tail domain (Fig. 3a). One of these latter mutations is located outside of the homodimerization domain, while the second (leading to a deletion of 4 AA) is located in a region required for binding of the associated light chains DYNC1L and DYNC1LI (Fig. 3a). Homology modelling of DYNC1H1 mutations showed that 3 are located on the surface of the

microtubule BD (Fig. 3c). We note that *in vitro* experiments have shown that a closely located mutation (p.R3384P) weakens microtubule binding (data from Carter and colleagues[26]; the residue is referenced as R3382).

We evaluated the effect of two of our newly discovered *DYNC1H1* mutations on microtubule binding. Wild type and mutant (p.K3336N and p.R3384Q) sequences containing the DYNC1H1 microtubule BD were fused with the antiparallel coiled-coil side arm contained in the native structure of seryl-tRNA synthetase[27] as C-terminally His_6-tagged proteins. This chimeric arrangement fixes the alignment of the two strands of the coiled-coil in their native conformation such that their registry results in a relatively high microtubule binding affinity[26]. The recombinant proteins were expressed in E. coli, affinity purified and tested for their ability to co-sediment with taxol-polymerized microtubules through sucrose cushions. This experiment showed a significant reduction in microtubule binding affinity of both p.K3336N and p.R3384Q mutations compared to the wild type control (Fig. 3d).

***TUBG*1 mutations**

Two patients with *TUBG1* mutations (P367: c.1160T>C, p.L387P, P388: c.275A>G, p.Y92C) share a complex MCD combining posteriorly predominant pachygyria (or agyria) and severe microcephaly (-4SD). The third but less severe case (P478: c.991A>C, p.T331P) showed posterior pachygyria and laminar heterotopia with a thick and dysmorphic corpus callosum (Fig. 4b and Supplementary Table 4). *TUBG1* is one of two human genes encoding γ-tubulin[28] and is highly expressed in foetal brain. The protein is a structural component of the centrosome and associates with at least 6 other proteins to form the γ-tubulin ring complex (γTuRC), which functions in microtubule nucleation[29]. Two of the mutated residues (p.T331 and p.L387) are located in buried sites in two distinct α-helices (Fig. 4c); their mutation to proline residues is likely to destabilize these helices. One of these residues (p.T331) is located in the γ-γ interaction domain; the conserved mutated residue (p.Y92) is located in the vicinity of the GTP binding site (Fig. 4c)

The events leading to the assembly of the γTuRC are unknown. However, γ-tubulin, in common with the components of the α/β-tubulin heterodimer, requires facilitated folding by the cytosolic chaperonin CCT, and is discharged from it as a monomer[30]. We therefore assessed the effect of two of the γ-tubulin mutations (p.Y92C and p.L387P) on facilitated folding and on the structural stability of the monomer *in vitro*. The latter experiment showed that the integrity of the recombinant proteins is not significantly affected by either of the disease-associated mutations (Supplementary Fig. 6). On the other hand, we found a diminished yield of material migrating as monomeric γ-tubulin in the case of p.L387P with a corresponding increase (relative to wild type) of radioactivity migrating as an undischarged binary complex with CCT (Fig. 4d). These data suggest that the chaperonin-dependent folding (and hence the yield) of monomeric γ-tubulin is compromised by the p.L387P mutation. The effect of the p.Y92C mutation on facilitated folding via interaction with chaperonin is less evident (Fig. 4d), and it therefore seems likely that this mutation (and perhaps to some extent the others) exert their influence via the assembly and/or functional integrity of the γTuRC.

We analysed the consequences of our newly discovered disease-causing γ-tubulin mutations in vivo in two ways. First, we investigated the phenotype in yeast (S. cerevisiae) cells in which these mutations had been introduced into the conserved (although non-identical) residues in the single yeast γ-tubulin gene *tub4* (Supplementary Fig. 7a). All our mutant heterozygous and homozygous strains were viable. However, although we found no change in microtubule plus-end dynamics (Supplementary Table 6), tub4-W92C cells displayed an enhancement in the number and average maximal length of astral microtubules, as well as a decrease in the frequency of nucleation of new microtubules from the spindle pole body (SPD) (Supplementary Table 7 and Supplementary Fig. 7b). Moreover, we found abnormal mitotic features in a significant number of cells (tub4-W92C, 23%; tub4-V387P, 8%), consistent with incorrect nuclear positioning and reflecting a defect in mitotic microtubule organization (Fig. 5a and Supplementary Table 7). These data are consistent with both the disease-causing γ-tubulin mutations having a deleterious effect on critical aspects of microtubule behaviour, and with the more severe clinical phenotype associated with the p.W92C mutation. Second, we used *in utero* RNA interference to analyse the consequences of *Tubg1* downregulation on cortical radial neuronal migration in mice. We found that brain sections of E18.5 embryos that had been

electroporated 4 days previously with shRNA targeting *Tubg1* showed a significant fraction of RFP-positive cells in the subventricular zone/intermediate zone (SVZ/IZ), suggesting that *Tubg1* down-regulation induced a significant arrest of migrating cells (Fig. 5b, shTubg1). In contrast, embryos transfected identically *in utero* with RFP alone showed strong labelling in the cortical plate (Fig. 5b, Tomato). Expression of scrambled-sh controls had no effect on migration (Fig. 5b, Scramble), while shRNAi-induced neuronal migration defects were significantly rescued by overexpression of a wild type human *TUBG1* cDNA (Fig. 5b, Rescue)). Quantification of these effects is shown in Figure 5c. We repeated these *in utero* RNAi experiments using a second shRNA targeting the coding sequence, and found that it also affected neuronal radial migration, although the positions of misplaced cells appeared more disperse than with the first shRNA (data not shown). This observation is likely to be attributable to the fact that down-regulation of Tubg1 expression using the first shRNA is more efficient than in the case of the second shRNA (data not shown). We conclude that TUBG1 plays a critical role in neuronal migration during corticogenesis.

Discussion

Among 16 patients analysed by WES, mutations in 4 genes, *KIF5C, KIF2A, DYNC1H1* and *TUBG1,* encoding proteins that interact with microtubules were identified in a subset of 7 patients. The remaining 9 patients include (i) 4 in whom all tested variants were inherited from one of the healthy parents, and (ii) 5 with *de novo* events predicted to alter protein functions but with no clear link to microtubules (Supplementary Table 8). Further screening and re-evaluation of MRI data showed that mutations in*KIF5C, KIF2A, DYNC1H1* and *TUBG1*, are involved in a wide range of cortical and gyral pattern abnormalities associated with microcephaly, callosal, cerebellum, or brainstem dysgenesis (summarized in Supplementary table 4). First, in the familial form of severe MCD, P20 (Fig. 1) described here, we obtained convincing evidence for the presence of a maternal mosaic germline mutation in *KIF5C* that is responsible for the recurrence of the disease in four male patients. There is now a wide range of disorders for which the occurrence of parental germline mosaicism has been reported[31]. Indeed, with the recent application of DNA sequencing to whole genomes and whole exomes, the frequency of somatic and germline mosaicism may turn out to be higher than is currently appreciated. Our results highlight both the contribution of germline mosaic mutational events in families with recurrent genetic disorders and the power of whole exome sequencing to resolve these situations. For KIF5C,

we note that a recent report documented a *de novo* mutation in a sporadic patient with severe ID and microcephaly for whom MRI data were not available[32]. Second, patients with mutations in *KIF2A* and *TUBG1* share microcephaly and a cortical gyration pattern that more severely affects the posterior cortex. This gyration pattern is reminiscent of the LIS-1 related cortical gyration pattern[33]. Third, mutations in *DYNC1H1* are the cause of a wide spectrum of cortical malformations characterized mainly by posterior pachygyria (8/11, Supplementary Table 4). Some patients with mutations in *DYNC1H1* had evidence of additional abnormalities including microcephaly, nodular heterotopia, hypoplasia of the corpus callosum and dysmorphy of the basal ganglia, as well as evidence of peripheral neuropathy (3/11). However, the most striking finding is the concomitant presence in two patients of both pachygyria and PMG patterns (Supplementary Table 4, P122 and P217 and Fig. 3), traditionally regarded as distinct entities. This association has also been reported in WDR62-related disorders[11] that include patients with microcephaly, PMG and schizenccephaly.

Interestingly, missense mutations in DYNC1H1 have been primarily associated with neuropathy: an axonal dominant form of Charcot-Marie-Tooth disease (CMT2)[25], and a dominant form of spinal muscular atrophy[24,34]. More recently, Willemsen and colleagues reported *de novo* missense mutations in *DYNC1H1* in two patients with intellectual disability and signs of cortical malformations[32,35]. Taken together, these data indicate that heterozygous missense mutations in *DYNC1H1* underlie a broad phenotypic spectrum extending from peripheral neuropathies to cerebral malformations. However, *DYNC1H1* is emerging as an important and principal locus for mutations responsible for MCD, and its screening should be recommended in unexplained and difficult to classify pachygyria/lissencephaly and PMG with or without microcephaly.

The data reported here extend the association between microtubule-based cellular processes and proper cortical development[8,9,36,37] to γ-tubulin and the microtubule-dependent motor proteins KIF5C, KIF2A and DYNC1H1. As for α- and β-tubulin isotypes (TUBA1A, TUBB2B, TUBB3 and TUBB5), all mutations identified so far in the genes encoding these proteins are heterozygous missense mutations. In the absence of loss-of-function mutations (i.e., nonsense, frameshift, splice, or genomic deletions), such mutations favour dominant negative effects rather than haploinsufficiency as primary molecular mechanisms that cause disease.

This hypothesis is further supported by our cellular data regarding the behaviour of mutant forms of KIF5C and KIF2A. It is nonetheless possible that haploinsufficiency could also contribute to functional defects of MCD-related proteins.

Our phenotypic evaluation of S. cerevisiae strains harbouring disease-causing mutations in Tub4 as well as our *in utero* suppression experiments suggest that adequate expression of *Tubg1* is required for normal microtubule behaviour and proper neuronal migration. Previous studies - including analyses of *kif2a-/-* and *Kif5c-/-* mice[19,38]- imply that sufficient expression of functional KIF5C, KIF2A and DYNC1H1 proteins is also required for proper cortical development. In the case of *DYNC1H1*, inactivation of the mouse homologue is embryonic lethal[39], while ENU-induced mouse mutants harbouring heterozygous missense mutations in the tail domain (*Legs at odd angles* (*Loa,* p.F580Y) and *Cramping 1* (*Cra1,* p.Y1055C) mainly result in early onset progressive neurodegenerative diseases[40]. This analysis also revealed defects in retrograde axonal transport[40] and defects in hippocampal neocortical lamination and neuronal migration[41]. In line with these results, Shu et al., reported that *in vivo* RNAi-mediated down-regulation of *Dync1h1* impairs neuronal migration and positioning in the developing neocortex[42].

Our data strongly suggest that the regulation of microtubule-dependent mitotic processes in progenitor cells, as well as the trafficking activities of the microtubule-dependent molecular motors *KIF2A*, *KIF5C*, and *DYNC1H1* in post-mitotic neuronal cells, are collectively essential for correct neuronal development (Supplementary Fig. 8). In light of this conclusion, it is understandable that functional disruption of any of these genes can lead to devastating defects in neuronal polarization, migration and differentiation.

Data accession numbers

Human *TUBG1 (*NM_001070), human *KIF5C* (NM_004522), human *DYNC1H1* (NM_001376), human KIF2A (NM_001098511), mouse *Tubg1* (NM_134024), human *DCX* (NM_181807), human *LIS1* (RefSeq NM_000430), human *ARX* (NM_139058), human *TUBA1A* (NM_006009), human *TUBB2B* (NM_178012), human *TUBB3* (NM_006086), human *GPR56* (NM_201524).

Acknowledgements

We are grateful to the patients and their families for their participation. We thank Franck J Fourniol and members of the Chelly lab for their thoughtful comments. We thank Dr. Ian Gibbons and Dr. Andrew Carter for generously providing the seryl tRNA synthetase dynein heavy chain fusion constructs used in the experiments described in this paper. We also thank members of the Cochin Hospital Cell Bank, the Centre National de Genotypage, Genoscope, Paris Descartes Bioinformatics platforms and Cochin Insitute genomic platform for their technical and bioinformatic assistance. This work was supported by funding from INSERM, Fondation pour la Recherche Médicale (FRM funding within the frame of the programme Equipe FRM – J Chelly), Fondation JED, Fondation maladies rares, Agence National de Recherche (ANR Blanc 1103 01 - project R11039KK; ANR E-Rare-012-01 – projet E10107KP) and the EU-FP7 project GENECODYS , grant number 241995. This work was also supported by a grant (GM097376 to NJC) from the NIH.

Author contribution statement

J.C. coordinated and instigated the study with N.J.C. K.P and N.L. analyzed whole exome sequencing data and performed genetic and molecular studies. L.B. and Y. S. performed and analyzed *in utero* RNAi experiments. F.F. provided technical assistance for *in utero* RNAi experiments. N.B.B., R.G. coordinated collection of clinical and imaging data, and D.G., E.F., F.D., C.C., M.B., D.B., B.D.B., S.N., C.G., P.P., V.d.P., J.M.P and V.L. helped in selecting patients. S.V., B.S.P., M.O. analyzed variations in candidate genes and screened subjects' DNA. G.T. and N.J.C. performed the biochemical studies. C.B. and A.A. performed the yeast studies. L.C.P. performed all DNA extractions from patient samples. P.N., T.T., C.M. performed bioinformatics analysis of exome sequencing data. D.Z. coordinated the whole exome sequencing procedure (library generation, exome enrichment and whole exome sequencing). J.C and N.J.C. drafted and finalized the manuscript, with the help of KP, NL, LB and YS.

Figure Legends

Figure 1. Recurrent severe MCD resulting from a germline mosaic mutation in *KIF5C* and analysis of mutant KIF5C ATPase activity and cellular localization

(a) Pedigree of the P20 family with four affected male individuals exhibiting severe MCD (Supplementary Fig. 3d), (b) Linear schematic representation of the KIF5C showing the position of the mutation (c) 3D model of the rat kinesin dimer (generated by pyMol [pdb: 3kin]) showing the p.E237 residue (red) located at the motor domain surface. (d) microtubule binding assay of recombinant wild type and mutant KIF5C proteins. Upper part shows analysis of sedimented microtubules by SDS-PAGE (as loading controls); the lower part shows autoradiographs of the same gels. Note that the p.E237V mutation does not appreciably affect the protein's ability to bind to microtubules. (e) Kinetics of microtubule-dependent ATP hydrolysis by wild type and mutant KIF5C proteins. The production of P_i was measured kinetically in reactions containing taxol-stabilized microtubules, an equal amount of purified recombinant KIF5C protein, and ATP using the malachite green colorimetric reaction. Diamonds and crosses represent wild type and mutant (p.E237V) proteins, respectively. Each time point represents the average of 6 experiments, +/- S.D. Note the complete absence of detectable ATP hydrolysis in the case of the p.E237V mutant protein. (f) Subcellular localization of transfected wild type and p.E237V mutant KIF5C in COS7 cells. KIF5C immunostaining (green) reveals a diffuse cytoplasmic distribution of wild type KIF5C with enrichment, as fluorescent puncta, along microtubules and in cortical regions of the cell, while mutant KIF5C heavily co-localises with and decorates microtubules (identified by α-tubulin labelling, shown in red) throughout the cell, but does not appear as puncta or accumulate in cortical clusters. Dapi was used as a counterstain to highlight nuclei. Scale bar 20 μm.

Figure 2. Mutations in *KIF2A* cause posterior predominant agyria/pachygyria and compromise productive folding and cellular localization

(a) Brain MRIs of patients with *KIF2A* mutations. Representative T1-Sagittal (first line), T2-axial (second line) and T2-coronal (third line) MRIs performed at 5 weeks in patient P147 and at 3 weeks in patient P462. Patient P147 (left hand column) shows posterior predominant agyria pachygyria, with a thick cortex and a thin corpus callosum. Patient P462 (right hand column) has posterior predominant pachygyria with subcortical

band heterotopias (arrows) and a thin corpus callosum. (b-c) Linear and 3D ribbon (pdb: 2gry) representations of the kinesin 2A polypeptide showing the position of the two heterozygous MCD-associated mutations (shown in red and pink) near the nucleotide binding site (shown in orange). (d) Folding of KIF2A. Wild type and mutant (p.S317N, p.H321D) forms of the KIF2A nucleotide binding domain (amino acids 126 – 526) were expressed in E. coli as recombinant C-terminally His_6-tagged proteins. Soluble extracts of host cells, the insoluble (particulate) fraction, and products that either failed to bind (non-binding) or bound and eluted (eluted) from columns of solid phase-bound Co^{++} were analysed by SDS-PAGE and (in the case of the affinity purified material) by Western blotting with an anti-His_6 antibody. Arrow identifies the recombinant KIF2A nucleotide binding domain. The location of molecular mass markers is shown at the left. (e-f) Immunofluorescence staining of KIF2A (green) and α-tubulin (red) in either COS7 cells transfected with WT or mutant (p.S317N and p.H321D) KIF2A cDNA constructs (e) or in wild type and p.H321D patient-derived fibroblasts (f). Note that instead of the expected diffuse punctiform cytoplasmic and nuclear distribution (as observed for wild type KIF2A), KIF2A mutants showed a predominant co-localization with and decoration of microtubules. In cells expressing high levels of mutant forms of KIF2A, the decorated microtubule-network is mainly in the central region of the cells and around the nucleus with a disorganized and bundled appearance of microtubules. The nuclear distribution is also disrupted, and in the case of both mutants, the nucleus appears free of KIF2A. A similar altered distribution of KIF2A is evident in patient-derived fibroblasts. Scale bar 20 mm.

Figure 3. Spectrum of MCD associated with mutations in *DYNC1H1* and analysis of the ability of mutant DYNC1H1 to bind to microtubules

(a) Schematic representation of DYNC1H1 protein showing the position of mutations causing MCD. (b) Brain MRI illustrations showing the phenotypic spectrum associated with *DYNC1H1* mutations. Top line, P122: Axial T1-weighted images showing diffuse coarse PMG, most prominent in the perisylvian region (arrow head). In frontal regions, PMG has the appearance of a dysmorphic cortex (*). The sagittal T2-weighted section shows a dysmorphic thick corpus callosum and hypoplasic brainstem. Second line, P535: Axial T1-weighted images showing a simplified gyral pattern on both frontal regions (arrow heads), large and dysmorphic basal ganglia and parieto-occipital pachygyria (asterisks). Sagittal T1 weighted image shows a

thick and dysmorphic corpus callosum. Third line, P398: Axial T1-weighted images showing bilateral frontal PMG (asterisks) with multiple small gyri giving an appearance of delicate PMG. (c) Illustration of the structure of the DYNC1H1 MTBD (ellipses) and the distal portion of the coiled-coil stalk of mouse cytoplasmic dynein as a fusion with seryl tRNA-synthetase (SRS, solid circle) from *Thermus thermophilus* (pdb: 3err). The Figure shows the surface location on the microtubuleBD of p.K3336, p.R3344 and p.R3384 residues. (d) Effect of dynein heavy chain mutations on binding to MTs. Left panel: Coomassie stain of purified ^{35}S-labeled wild type and mutant-containing seryl tRNA synthetase-DYNC1H1 MTBD fusion proteins analysed by SDS-PAGE. Right panels: purified labelled recombinant proteins (as shown on the left) were tested for their ability to co-sediment through sucrose cushions either in the presence (+Tub) or absence (-Tub) of taxol-polymerized MTs. Labelled material contained in the supernatants (S) and pellets (P) was analyzed by SDS-PAGE. Note that in the case of the mutant proteins, the amount of label sedimenting with MTs is reduced to a level close to that present in control reactions done without added tubulin.

Figure 4. Mutations in *TUBG1* cause MCD with posterior predominant pachygyria and analysis of the effect of γ-tubulin mutations on facilitated folding

(a) Linear representation of the TUBG1 protein showing the localization of the GTP binding site and TUBG1 mutations. (b) Brain MRI illustrations of patients with mutations in *TUBG1*. Top line: Axial T1-weighted images in 3 different patients (respectively, P388, first column; P478 second column, and P367, third column) with different *TUBG1* mutations show different degrees of pachygyria, with a thick cortex, most prominent in parieto-occipital regions (white asterisk). In the less severe case, pachygyria is milder with an aspect of posterior subcortical band heterotopia (red asterisk). Second line: Sagittal T1-weighted section showing a dysmorphic thick corpus callosum. Note that in the 3 cases, the cerebellum and brainstems are normal. (c) 3D model of the TUBG1 dimer (pdb: 3Cb2) showing the localization of the three mutated residues and the bound GTP molecule (yellow). (d) Effect of γ-tubulin mutations on facilitated folding. Sequences encoding full-length wild type and mutant (p.Y92C, p.L387P) γ-tubulin were expressed as ^{35}S-labeled proteins in reticulocyte lysate and the reaction products analyzed by gel filtration on Superose 6. Fractions emerging from the column were subjected to SDS-PAGE and the radioactivity migrating as γ-tubulin quantified using a phosphorimager. Note the diminished yield of material migrating as monomeric γ-tubulin in the case of

p.L387P, with a corresponding increase (relative to wild type) of radioactivity migrating as a binary complex with the cytosolic chaperonin (the CCT binary complex has the same apparent mass as the largest molecular mass marker, thyroglobulin, indicated by the black arrowhead). Arrows mark the elution position of molecular mass standards (thyroglobulin [black; 670kDa], IgG [orange; 158kDa], ovalbumin [purple; 44kDa], myoglobin [red; 17kDa]) run under identical conditions.

Figure 5: **TUBG1 mutations affect mitotic figures in yeast cells and suppression of expression of *Tubg1* disrupts neuronal migration in the developing mouse neocortex**

(a) Yeast mitotic figures of γ-tubulin disease-related substitutions. At least 100 cells were examined in each strain after transformation with GFP-Bik1p, an α-tubulin binding protein that labels mitotic spindle and astral microtubules. The percentage of large budded cells with nuclei and microtubule positions were scored in the different strains as indicated. ***p<0.001 c2 test comparisons. (b) Validated shRNAs that suppressed *Tubg1* expression in cultured N2A cells by approximately 50-60% were co-electroporated with an RFP-encoding reporter construct (Tomato) into progenitors cells located in the ventricular zone (VZ) of E14.5 mouse neocortices. The Figure shows examination of coronal sections of mouse brains 4 days after electroporation at E14.5 with an RFP-encoding vector (Tomato), control shRNA (Scramble), *Tubg1* shRNA or *Tubg1* shRNA in combination with pCMV6-*Tubg1* (Rescue). (c) Fluorescence intensities reflecting distribution of electroporated cells within the cortex were converted into gray values and measured from the VZ to the MZ. Bars represent the mean ± SEM of fluorescence intensities in 10 equal strata (stratum 1 corresponding to the VZ and stratum 10 to the MZ) dividing the cortex of independent brains (Tomato n=4, Scramble n=3, sh *Tubg1* n=11, Rescue n=2). Note that sh *Tubg1* knockdown leads to an increase in the percentage of transfected cells located in the SVZ/IZ (strata 3 and 4) and a significant decrease in the upper layers of the CP (strata 9 and 10) compared with the Scramble control. Cells transfected with sh *Tubg1* and pCMV6-*Tubg1* have mainly reached the upper layers of the CP (strata 8 to 10), showing that migration disruption is a specific consequence of *Tubg1* RNAi. Student *t* test : *p < 0.1, **p < 0.01 and ***p < 0.001. Scale bar: 100μ**m.**

Table 1. Summary of *KIF5C, KIF2A, TUBG1* and *DYNC1H1* mutations.

Patient	Gene	CDNA variation	Protein variation	Transmission
P20	*KIF5C*	c.710A>T	p.E237V	Maternal mosaicism
P462	*KIF2A*	c.961C>G	p.H321D	*De novo*
P147	*KIF2A*	c.950G>A	p.S317N	*De novo*
P367	*TUBG1*	c.1160T>C	p.L387P	*De novo*
P388	*TUBG1*	c.275A>G	p.Y92C	*De novo*
P478	*TUBG1*	c.991A>C	p.T331P	Father's DNA unavailable
P144	*DYNC1H1*	c.del1976-1987	p.del659-662	*De novo*
P582	*DYNC1H1*	c.386A>T	p.K129I	*De novo*
P122	*DYNC1H1*	c.10008G>T	p.K3336N	*De novo*
P217	*DYNC1H1*	c.10151G>A	p.R3384Q	*De novo*
P398	*DYNC1H1*	c.4700G>A	p.R1567Q	*De novo*
P535	*DYNC1H1*	c.10031G>A	p.R3344Q	*De novo*
360J	*DYNC1H1*	c.5884C>T	p.R1962C	*De novo*
346D	*DYNC1H1*	c.9722A>C	p.K3241T	Familial
574C	*DYNC1H1*	c.10031G>A	p.R3344Q	*De novo*

ONLINE Methods

Patients

Patients and parents' blood samples were obtained according to local institutional review boardsguidelines. 16 cases were selected with either LIS (6 patients) or PMG (10 patients) in association with at least one of the following features: microcephaly, dysgenesis of the cerebellum, brainstem, basal ganglia or corpus callosum. Patients with LIS included those with agyria, pachygyria or subcortical laminar heterotopia, and those with PMG included perisylvian, frontal, diffuse, and multifocal PMG.

An additional cohort of 162 patients comprising 80 patients with PMG, 58 with LIS and 24 with predominant posteror pachygyria, was used to perform extensive screening of candidate genes. It included 57 patients with microcephaly, 74 with dysgenesis or agenesis of the corpus callosum, 18 with dysmorphic basal ganglia, and 38 with cerebellar vermian and /or hemispheric hypoplasia or dysplasia.

All patients' DNAs were analyzed by CGH-microarray using the NimbleGen chip 720,000-probes (720 K) array (Roche-NimbleGen, Madison, WI) to exclude potential pathogenic CNVs. Metabolic screening was performed to exclude metabolic disorders. Likewise, screening of the coding regions of *DCX* (RefSeq NM_181807), *LIS1* (RefSeq NM_000430), *ARX* (RefSeq NM_139058), *TUBA1A* (RefSeq NM_006009), *TUBB2B* (RefSeq NM_178012), *TUBB3* (RefSeq NM_006086) or *GPR56* (RefSeq NM_201524)[43-46] was performed to exclude pathogenic mutations.

Genotyping

High-throughput microarray genotyping of approximately 262,000 SNPs was performed using one array (version NspI*)* from the Affymetrix GeneChip® Human Mapping 500K Array set (Affymetrix, Santa Clara, CA, USA). The recommended protocol as described in the Affymetrix manual was followed.

Whole exome sequencing and analysis

Library generation, exome enrichment and whole exome sequencing were performed at the French National Centre for Genotyping (CNG, Evry, France). Briefly, libraries were prepared from 3 µg genomic DNA was extracted from whole blood using an optimized SureSelect Human Exome kit (Agilent, Santa Clara, CA,

USA) following the manufacturer's instructions. Captured, purified and clonally amplified libraries targeting the exome were then sequenced on a HiSeq 2000 (Illumina, San Diego, CA, USA) according to the manufacturer's recommendations. Obtained sequence reads were aligned to the human genome (hg19) using BWA software[15]. Downstream processing was carried out with the Genome analysis toolkit (GATK[47,48], SAMtools[49] and Picard Tools (http://picard.sourceforge.net). Single-nucleotide variants and indels were subsequently called by the SAMtools suite (mpileup, bcftools, vcfutil). All calls with a read coverage ≤5x and a Phred-scaled SNP quality of ≤20 were filtered out. Substitution and variation calls were made with the SAMtools pipeline (mpileup). Variants were annotated with an in-house Paris Descartes bioinformatics platform pipeline based on the Ensembl database (release 67)[50].

Variations validation and gene screening

After exome analysis, each selected variant was confirmed by PCR and direct sequencing using parents and patient's DNA. For each patient, the complete *TUBG1 and KIF5C* coding sequences (respectively RefSeq NM_001070 and NM_004522) and splice sites, as well as exons corresponding respectively to the AAA1 and the stalk domains of *DYNC1H1* (RefSeq NM_001376), were amplified in independent PCR reactions from genomic DNA and sequenced using BigDye dideoxyterminator chemistry and a ABI3700 DNA analyzer (Applied Biosystems, Foster City, CA, USA). Primer sequences and positions, PCR conditions and product sizes are available upon request.

Protein modelling

Amino acid substitutions were plotted on solved protein structures for rat kinesin, the human KIF2A nucleotide binding domain, human TUBG1 and the mouse Dync1h1 stalk domain in fusion with seryl-tRNA synthetase from Thermus thermophilus using PyMOL software (http///www.pymol.org/). Models were built by homology modeling using Research Collaboratory for Structural Bioinformatics PDB codes: 3kin, 2gry, 3Cb2 and 3err. Images in Figure 1 to Figure 4 were rendered using PyMOL.

Cloning, expression and *in vitro* translation

A plasmid containing the full-length sequence encoding KIF5C was provided by Pr F. A.Stephenson, School of Pharmacy, University of London. A sequence encoding the N-terminal 380 amino acids of KIF5C containing a C-terminal His_6 tag was generated from this clone by PCR. Sequences encoding full-length

human γ-tubulin were from Dr. B. R. Oakley[30]. A sequence encoding the DYNC1H1 MTBD was obtained by PCR using a human brain cDNA library (Clontech, Mountain View, CA,USA) as template and inserted into the seryl-tRNA synthetase 12 heptad-containing α-registry fusion construct described by Carter et al.[26] (GeneBank Accession Number FJ039866). Mutations were introduced by site-directed mutagenesis using the QuickChange II kit (Stratagene, Santa Clara, CA, USA). For experiments requiring expression *in vitro*, sequences were inserted into the pET23b vector (Novagen, EMD Millipore Germany) and used to drive expression in either rabbit reticulocyte lysate (TNT, Promega, Madison, WI, USA) containing ^{35}S-methionine, or in *E. coli* BL21DE3 pLysS in which synthesis of endogenous *E. coli* proteins was suppressed by incubation in the presence of rifampicin[51]. In bacterial expression experiments, lysis was effected 2 h post-induction with IPTG by two successive cycles of freezing and thawing, followed by incubation with DNAse I and centrifugation as previously described[52]. Affinity purification of His_6-tagged proteins from the resulting supernatants was done using solid phase-bound Co^{++} beads using the protocol recommended by the manufacturer (Clontech, Mountain View, CA, USA). The purity of expressed proteins was checked by SDS-PAGE. In some experiments, the integrity of *in vitro* translated wild type and mutant forms of γ-tubulin was assessed by measuring its susceptibility to digestion with proteinase K as described[53].

Gel filtration analyses

The migration properties of recombinant wild type and mutant forms of KIF5C sequences containing the motor domains and a portion of the stalk domain was assessed on a column (1.0 x 30cm) of Superose 6 via FPLC (GE, Uppsala, Sweden) run in 20 mM Na phosphate buffer, pH 7.2 containing 0.1M NaCl, 0.5 mM EGTA and 1 mM DTT (buffer K). The products of *in vitro* TNT reactions done in rabbit reticulocyte lysate (10 ul) were diluted with 0.1 ml of buffer K supplemented with 20 uM GTP, and centrifuged for 15 mins at 100,000 x g at 4^0C to remove all particulate material. The resulting supernatant was applied to the Superose 6 column equilibrated and run in buffer K containing 20 uM GTP and 5% v/v glycerol. Radioactivity contained in 0.5 ml fractions were measured in 20 ul aliquots by scintillation counting, and further aliquots were analyzed by SDS-PAGE and autoradiography. Radioactivity contained in the band corresponding to γ-tubulin was quantified using a phosphorimager.

Measurement of rates of ATP hydrolysis

ATP hydrolysis by recombinant WT and p.E237V mutant KIF5C forms was measured in 20ul reactions containing 1.0 pmole of purified protein in 20 mM PIPES buffer, pH 6.9, 1.0 mM $MgCl_2$, 0.5 mM ATP and 1.0 mg (measured as total protein) of taxol-polymerized microtubules. Reaction mixtures were incubated at 30^0C. At various intervals, aliquots (2.0 ul) were withdrawn and the P_i content measured using the malachite green phosphomolybdate assay[54].

Microtubule binding assays

MTs purified from bovine brain[55] were depolymerized in 20 mM Pipes, pH 6.9, 1 mM $MgCl_2$, 1 mM EGTA by incubation on ice and cleared by centrifugation at 60,000 x g for 10 mins. Purified ^{35}S-labeled KIF5C (in the range 0.2 – 6.9 nmoles) or ^{35}S-labeled chimeric seryl-tRNA synthetase containing the DYNC1H1 MTBD were added to reactions containing 2.0 mg/ml depolymerized tubulin, 1 mM GTP, 0.5 mM AMP-PNP and 20 mM taxol and the mixtures incubated at 30^0C for 20 mins. Reaction products were loaded onto cushions (0.25 ml) containing 1 M sucrose in 40 mM MES, pH 6.8, 0.5 mM $MgCl_2$, 0.5 mM EGTA, 0.5 mM GTP, 0.25 mM AMP-PNP and 10 mM taxol contained in 1.5 ml Eppendorff tubes, and centrifuged for 15 mins at 100,000 x g at 30^0C in a Beckman TL-100 rotor. The protein and radioactivity content of the resulting MT pellets (in the case of reactions done with bacterially expressed KIF5C proteins) or pellets and supernatants (in the case of experiments done with *in vitro* translated KIF5C and dynein heavy chain fragments) was determined following SDS-PAGE.

Folding of KIF2A nucleotide binding domains

Sequences spanning the centrally located nucleotide binding domain of human KIF2A (amino acids 126 - 526) were obtained by PCR using full-length cloned wild type (Origene, Rockville, MD, USA) or mutant-bearing cDNAs as template, and the products inserted in-frame with C-terminal His tag into the pET 23b vector using the Nde I and Not I sites. Proteins were expressed in E. coli BL21 DE3 cells following induction with 1.0 mM IPTG at an A_{600} of 1.0. 2.5 hours post induction, cells were harvested by centrifugation, washed by resuspension in 0.3M NaCl, 1 mM $MgCl_2$, 0.1 mM ATP, 50 mM HEPES buffer pH 7.5, and lysed by three brief pulses of sonication at 0^0C. A particle-free supernatant was obtained after two centrifugationsat 30,000 and 200,000 x g, at 4^0C. The supernatants were applied to columns of Talon cobalt affinity beads (Clontech, Mountain View, CA, USA); andeluted in imidazole-containing buffer. Samples were analyzed by 9% SDS-

PAGE and stained with Coomassie blue. In some cases, the gel content was transferred to nitrocellulose and probed with a mouse anti-His monoclonal antibody.

Cell Culture, Transfections and Immunofluorescence

PCMV6 plasmids containing either full length human *KIF2A* (SC117315) or *KIF5C* (RC218796) cDNAs were purchased from Origene . Mutations were introduced by site directed mutagenesis using a Quikchange II kit.

Constructs were transfected into COS-7 or human fibroblasts cells using a Neon transfection system (Lifetechnologies, Carlsbad, CA, USA) according to the manufacturer's instructions. Cells were then grown on glass coverslips in Dulbecco's Modified Eagle's Medium containing 10% (v/v) fetal calf serum. After paraformaldehyde fixation, immunostaining was performed with either a rabbit polyclonal anti-KIF2A (ab37005, Abcam Inc.) or an anti-KIF5C antibody (ARP54736, Avivasysbio, San Diego, CA, USA or ab5630, Abcam Cambridge, UK) (together with a mouse monoclonal anti-α-tubulin antibody (DM1A, Sigma-Aldrich, St. Louis, MO).

Yeast strains and plasmids

Yeast strains used in this study were Y20000 (*MAT***a**/*MAT***α**; *his3Δ 0/his3Δ 0; leu2Δ /leu2Δ 0; met15Δ 0/MET15; LYS2/lys2Δ 0; ura3Δ 0/ura3Δ 0*), all provided by EUROSCARF. The W92C and V387P mutations were obtained by direct mutagenesis of the *Tub4* gene carried by the plasmid pKanTUB4::LEU2, using the QuickchangeII kit and following the manufacturer's instructions.

Measurement of yeast MT dynamics *in vivo*

Cells were seeded and grown overnight in SD complete media at 30°C foolowing by a reseed at 30°C to mid-log phase. Cells were pelleted, resuspended in SD complete media , imaged on an Axio Image MI (Zeiss, Germany) microscope with a 100x Plan Fluor 1.4 N.A. objective, and captured using a Coolsnap HQ camera (Photometrics). A typical acquisition protocol acquired five z-series fluorescent images at 0.5 mm axial steps and one differential interference contrast (DIC) image corresponding to the central fluorescent image. Time-lapse image series were acquired at 10 s intervals during 10 minutes.

shRNA contructs

We conducted RNAi experiments using shRNA constructs commercially designed and provided by Origene. Four different 29-mer sequences cloned in the pGFP-V-RS vector and targeting mouse *Tubg1* (NM_134024) mRNA were used to identified the most efficient shRNA construct. A CAGGS-red fluorescent protein containing plasmid and a HuSH 29-mer non-effective (scrambled) were used as controls. Efficiency experiments were conducted in N2A cells, normalized by amplification of cyclophilin A and quantified by quantitative PCR using the SybrGreen master mix and a LC480 LightCycler instrument (Roche, Basel, Switzerland) according to the manufacturer's instructions.

In utero electroporation

Swiss mice (Janvier, Le Genest Saint Isle, France) were mated, maintained and used in our animal facilities in accordance with European Union and French legislation. Timed pregnant mice (E14.5) were anesthetized with isoflurane (2L/min 2/4% isoflurane; Minerve, Esternay, France). The uterine horns were exposed and a lateral ventricle of each embryo was injected via pulled glass capillaries and a microinjector (Picospritzer II; General Valve Corp) with Fast Green (2 µg/ml; Sigma) combined with the following DNA constructs: 0.5 mg/ml pCAGGS-red fluorescent protein (mRFP) either alone or together with 2 or 3µl of shRNA construct at 1.0 mg/ml targeting *TUBG1* mRNA (or scramble, or wild type cDNA). Plasmids were further electroporated on the head of the embryo by discharging a 4500 mF capacitor charged to 45 V with a CUY21EDIT electroporator (SonidelLtd, Raheny, Dublin) in five electric pulses of 50ms at 950 ms intervals. Embryonic mice were electroporated at E14.5 then brains were harvested after 4 days of development (E18.5), sectioned in 80µm slices using a VT1000S vibratome (Leica Microsystems, Reuil Malmaison, France) and maintained in 0.01% Azide-PBS buffer.

References

1. Caviness, V.S., Jr., Takahashi, T. & Nowakowski, R.S. Numbers, time and neocortical neuronogenesis: a general developmental and evolutionary model. *Trends Neurosci* **18**, 379-83 (1995).
2. Rakic, P. & Caviness, V.S., Jr. Cortical development: view from neurological mutants two decades later. *Neuron* **14**, 1101-4 (1995).
3. Francis, F. et al. Human disorders of cortical development: from past to present. *Eur J Neurosci* **23**, 877-93 (2006).
4. Guerrini, R., Dobyns, W.B. & Barkovich, A.J. Abnormal development of the human cerebral cortex: genetics, functional consequences and treatment options. *Trends Neurosci* **31**, 154-62 (2008).
5. Barkovich, A.J., Guerrini, R., Kuzniecky, R.I., Jackson, G.D. & Dobyns, W.B. A developmental and genetic classification for malformations of cortical development: update 2012. *Brain : a journal of neurology* **135**, 1348-69 (2012).
6. Ostergaard, P. et al. Mutations in KIF11 cause autosomal-dominant microcephaly variably associated with congenital lymphedema and chorioretinopathy. *Am J Hum Genet* **90**, 356-62 (2012).
7. Kousar, R. et al. Mutations in WDR62 gene in Pakistani families with autosomal recessive primary microcephaly. *BMC neurology* **11**, 119 (2011).
8. Jaglin, X.H. & Chelly, J. Tubulin-related cortical dysgeneses: microtubule dysfunction underlying neuronal migration defects. *Trends Genet* **25**, 555-66 (2009).
9. Tischfield, M.A., Cederquist, G.Y., Gupta, M.L., Jr. & Engle, E.C. Phenotypic spectrum of the tubulin-related disorders and functional implications of disease-causing mutations. *Current opinion in genetics & development* **21**, 286-94 (2011).
10. Breuss, M. et al. Mutations in the beta-Tubulin Gene TUBB5 Cause Microcephaly with Structural Brain Abnormalities. *Cell Rep* (2012).
11. Bilguvar, K. et al. Whole-exome sequencing identifies recessive WDR62 mutations in severe brain malformations. *Nature* **467**, 207-10 (2010).
12. Manzini, M.C. & Walsh, C.A. What disorders of cortical development tell us about the cortex: one plus one does not always make two. *Curr Opin Genet Dev* **21**, 333-9 (2011).
13. Veltman, J.A. & Brunner, H.G. De novo mutations in human genetic disease. *Nature reviews. Genetics* **13**, 565-75 (2012).
14. Vissers, L.E. et al. A de novo paradigm for mental retardation. *Nature genetics* **42**, 1109-12 (2010).
15. Li, Y. et al. Resequencing of 200 human exomes identifies an excess of low-frequency non-synonymous coding variants. *Nature genetics* **42**, 969-72 (2010).
16. Sindelar, C.V. & Downing, K.H. An atomic-level mechanism for activation of the kinesin molecular motors. *Proc Natl Acad Sci U S A* **107**, 4111-6 (2010).
17. Dunn, S. et al. Differential trafficking of Kif5c on tyrosinated and detyrosinated microtubules in live cells. *J Cell Sci* **121**, 1085-95 (2008).
18. Nakata, T. & Hirokawa, N. Point mutation of adenosine triphosphate-binding motif generated rigor kinesin that selectively blocks anterograde lysosome membrane transport. *J Cell Biol* **131**, 1039-53 (1995).
19. Homma, N. et al. Kinesin superfamily protein 2A (KIF2A) functions in suppression of collateral branch extension. *Cell* **114**, 229-39 (2003).
20. Kumar, P., Henikoff, S. & Ng, P.C. Predicting the effects of coding non-synonymous variants on protein function using the SIFT algorithm. *Nat Protoc* **4**, 1073-81 (2009).
21. Ramensky, V., Bork, P. & Sunyaev, S. Human non-synonymous SNPs: server and survey. *Nucleic Acids Res* **30**, 3894-900 (2002).
22. Hirokawa, N., Noda, Y., Tanaka, Y. & Niwa, S. Kinesin superfamily motor proteins and intracellular transport. *Nat Rev Mol Cell Biol* **10**, 682-96 (2009).
23. Poirier, K. et al. Expanding the spectrum of TUBA1A-related cortical dysgenesis to Polymicrogyria. *Eur J Hum Genet* (2012).
24. Harms, M.B. et al. Mutations in the tail domain of DYNC1H1 cause dominant spinal muscular atrophy. *Neurology* **78**, 1714-20 (2012).

25. Weedon, M.N. et al. Exome sequencing identifies a DYNC1H1 mutation in a large pedigree with dominant axonal Charcot-Marie-Tooth disease. *American journal of human genetics* **89**, 308-12 (2011).
26. Carter, A.P. et al. Structure and functional role of dynein's microtubule-binding domain. *Science* **322**, 1691-5 (2008).
27. Gibbons, I.R. et al. The affinity of the dynein microtubule-binding domain is modulated by the conformation of its coiled-coil stalk. *J Biol Chem* **280**, 23960-5 (2005).
28. Wise, D.O., Krahe, R. & Oakley, B.R. The gamma-tubulin gene family in humans. *Genomics* **67**, 164-70 (2000).
29. Kollman, J.M., Merdes, A., Mourey, L. & Agard, D.A. Microtubule nucleation by gamma-tubulin complexes. *Nat Rev Mol Cell Biol* **12**, 709-21 (2011).
30. Melki, R., Vainberg, I.E., Chow, R.L. & Cowan, N.J. Chaperonin-mediated folding of vertebrate actin-related protein and gamma-tubulin. *J Cell Biol* **122**, 1301-10 (1993).
31. Erickson, R.P. Somatic gene mutation and human disease other than cancer: an update. *Mutat Res* **705**, 96-106 (2010).
32. de Ligt, J. et al. Diagnostic Exome Sequencing in Persons with Severe Intellectual Disability. *N Engl J Med* (2012).
33. Dobyns, W.B. et al. Differences in the gyral pattern distinguish chromosome 17-linked and X-linked lissencephaly. *Neurology* **53**, 270-7 (1999).
34. Tsurusaki, Y. et al. A DYNC1H1 mutation causes a dominant spinal muscular atrophy with lower extremity predominance. *Neurogenetics* (2012).
35. Willemsen, M.H. et al. Mutations in DYNC1H1 cause severe intellectual disability with neuronal migration defects. *Journal of medical genetics* **49**, 179-83 (2012).
36. Higginbotham, H.R. & Gleeson, J.G. The centrosome in neuronal development. *Trends Neurosci* **30**, 276-83 (2007).
37. Wynshaw-Boris, A., Pramparo, T., Youn, Y.H. & Hirotsune, S. Lissencephaly: mechanistic insights from animal models and potential therapeutic strategies. *Semin Cell Dev Biol* **21**, 823-30 (2010).
38. Kanai, Y. et al. KIF5C, a novel neuronal kinesin enriched in motor neurons. *The Journal of neuroscience : the official journal of the Society for Neuroscience* **20**, 6374-84 (2000).
39. Harada, A. et al. Golgi vesiculation and lysosome dispersion in cells lacking cytoplasmic dynein. *J Cell Biol* **141**, 51-9 (1998).
40. Hafezparast, M. et al. Mutations in dynein link motor neuron degeneration to defects in retrograde transport. *Science* **300**, 808-12 (2003).
41. Ori-McKenney, K.M. & Vallee, R.B. Neuronal migration defects in the Loa dynein mutant mouse. *Neural Dev* **6**, 26 (2011).
42. Shu, T. et al. Ndel1 operates in a common pathway with LIS1 and cytoplasmic dynein to regulate cortical neuronal positioning. *Neuron* **44**, 263-77 (2004).
43. Keays, D.A. et al. Mutations in alpha-tubulin cause abnormal neuronal migration in mice and lissencephaly in humans. *Cell* **128**, 45-57 (2007).
44. Poirier, K. et al. Large spectrum of lissencephaly and pachygyria phenotypes resulting from de novo missense mutations in tubulin alpha 1A (TUBA1A). *Hum Mutat* **28**, 1055-64 (2007).
45. Jaglin, X.H. et al. Mutations in the beta-tubulin gene TUBB2B result in asymmetrical polymicrogyria. *Nat Genet* **41**, 746-52 (2009).
46. Poirier, K. et al. Mutations in the neuronal ss-tubulin subunit TUBB3 result in malformation of cortical development and neuronal migration defects. *Hum Mol Genet* **19**, 4462-73 (2010).
47. McKenna, A. et al. The Genome Analysis Toolkit: a MapReduce framework for analyzing next-generation DNA sequencing data. *Genome Res* **20**, 1297-303 (2010).
48. DePristo, M.A. et al. A framework for variation discovery and genotyping using next-generation DNA sequencing data. *Nat Genet* **43**, 491-8 (2011).
49. Li, H. et al. The Sequence Alignment/Map format and SAMtools. *Bioinformatics* **25**, 2078-9 (2009).
50. Flicek, P. et al. Ensembl 2012. *Nucleic Acids Res* **40**, D84-90 (2012).
51. Studier, F.W., Rosenberg, A.H., Dunn, J.J. & Dubendorff, J.W. Use of T7 RNA polymerase to direct expression of cloned genes. *Methods Enzymol* **185**, 60-89 (1990).
52. Gao, Y., Thomas, J.O., Chow, R.L., Lee, G.H. & Cowan, N.J. A cytoplasmic chaperonin that catalyzes beta-actin folding. *Cell* **69**, 1043-50 (1992).

53. Tian, G., Vainberg, I.E., Tap, W.D., Lewis, S.A. & Cowan, N.J. Specificity in chaperonin-mediated protein folding. *Nature* **375**, 250-3 (1995).
54. Bernal, C., Palacin, C., Boronat, A. & Imperial, S. A colorimetric assay for the determination of 4-diphosphocytidyl-2-C-methyl-D-erythritol 4-phosphate synthase activity. *Anal Biochem* **337**, 55-61 (2005).
55. Shelanski, M.L., Gaskin, F. & Cantor, C.R. Microtubule assembly in the absence of added nucleotides. *Proc Natl Acad Sci U S A* **70**, 765-8 (1973).

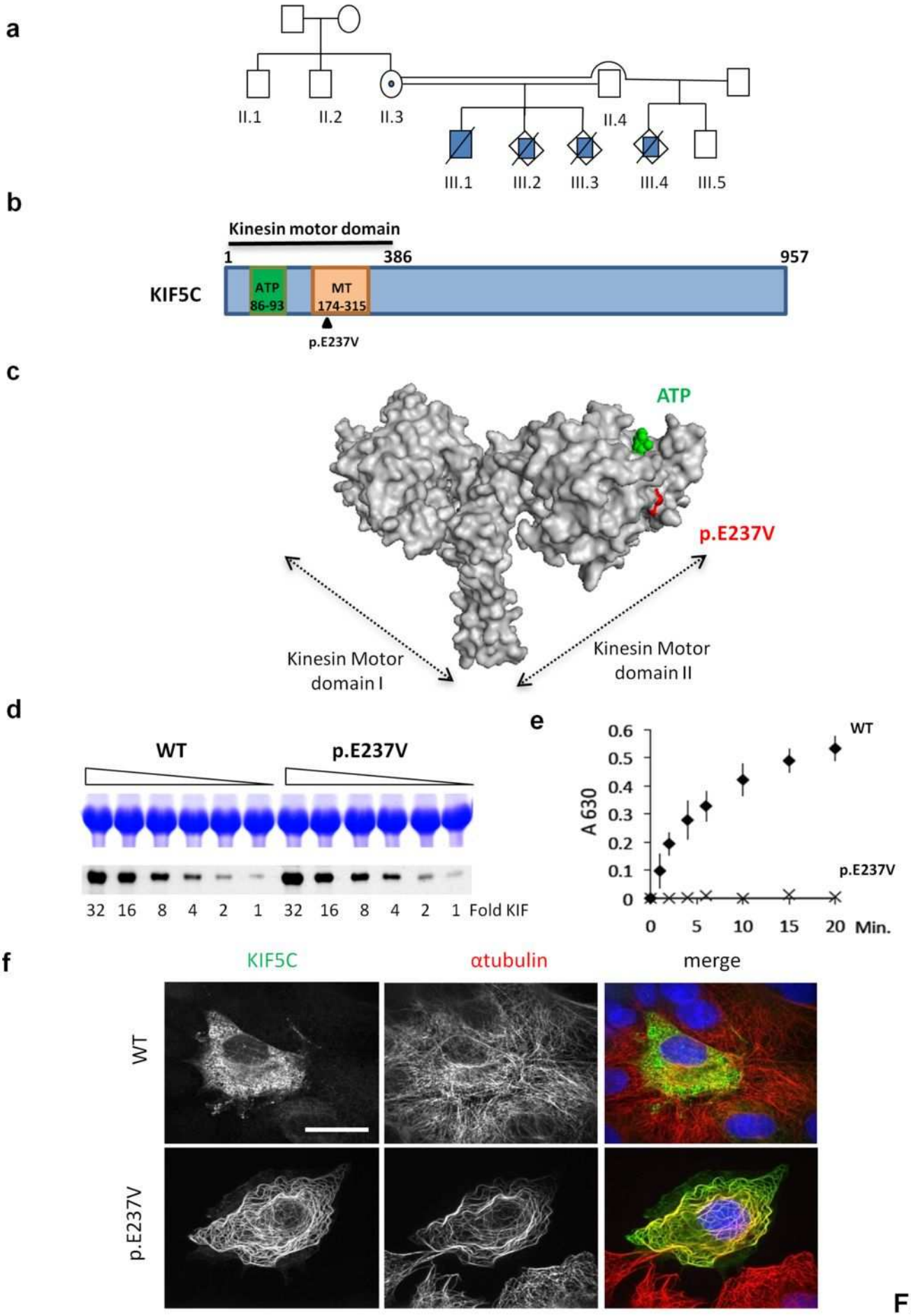
a
II.1
II.2
II.3
II.4
III.1
III.2
III.3
III.4
III.5
b
Kinesin motor domain
1
386
957
KIF5C
ATP
86-93
MT
174-315
p.E237V
c
ATP
p.E237V
Kinesin Motor
domain I
Kinesin Motor
domain II
d
WT
p.E237V
32 16 8 4 2 1 32 16 8 4 2 1 Fold KIF
e
A 630
0.6
0.5
0.4
0.3
0.2
0.1
0
WT
p.E237V
0 5 10 15 20 Min.
f
KIF5C
αtubulin
merge
WT
p.E237V

Figure 1

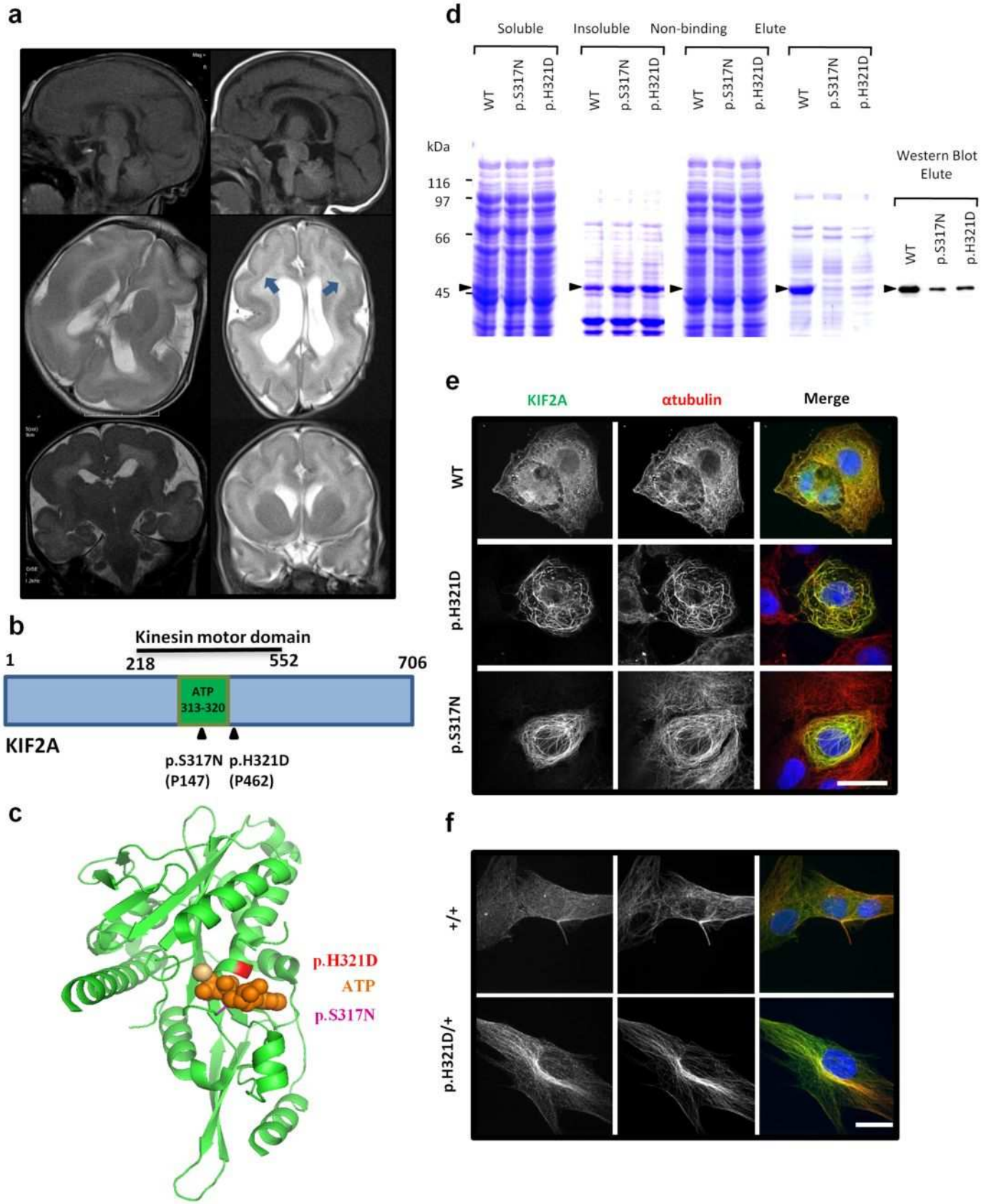
a
b
Kinesin motor domain
1
218
552
706
ATP
313-320
KIF2A
p.S317N
(P147)
p.H321D
(P462)
c
p.H321D
ATP
p.S317N
d
Soluble
Insoluble
Non-binding
Elute
WT
p.S317N
p.H321D
kDa
116
97
66
45
Western Blot
Elute
e
KIF2A
αtubulin
Merge
WT
p.H321D
p.S317N
f
+/+
p.H321D/+

Figure 2

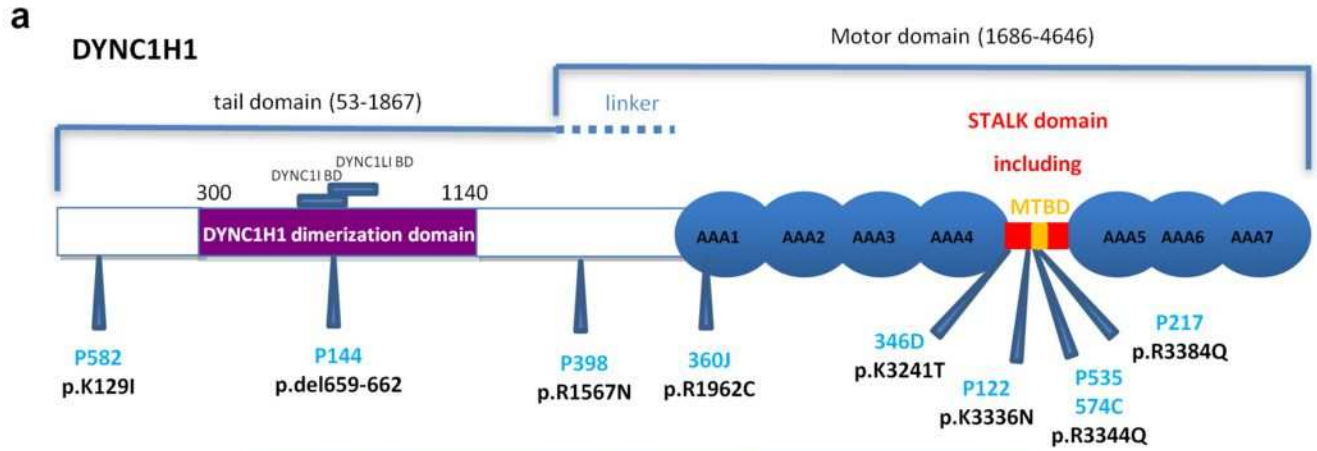
a
DYNC1H1
Motor domain (1686-4646)
tail domain (53-1867)
linker
STALK domain
including
DYNC1I BD
DYNC1LI BD
300
1140
MTBD
DYNC1H1 dimerization domain
AAA1
AAA2
AAA3
AAA4
AAA5
AAA6
AAA7
P582
p.K129I
P144
p.del659-662
P398
p.R1567N
360J
p.R1962C
346D
p.K3241T
P122
p.K3336N
P535
574C
p.R3344Q
P217
p.R3384Q

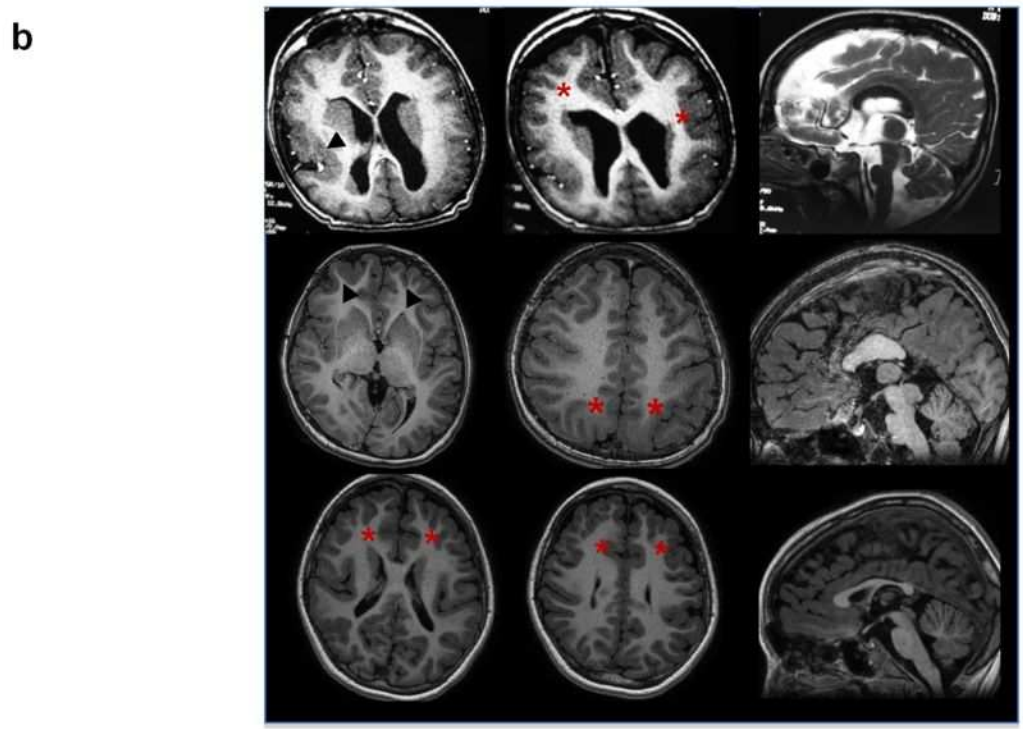
b

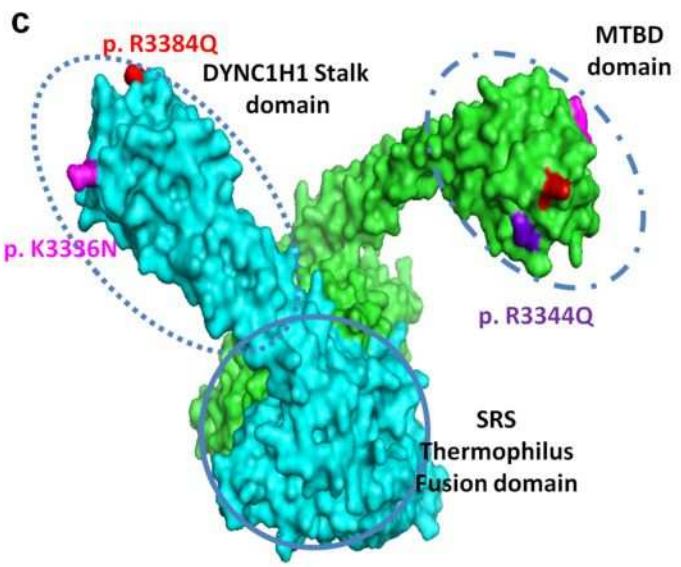
c
p. R3384Q
DYNC1H1 Stalk
domain
MTBD
domain
p. K3336N
p. R3344Q
SRS
Thermophilus
Fusion domain

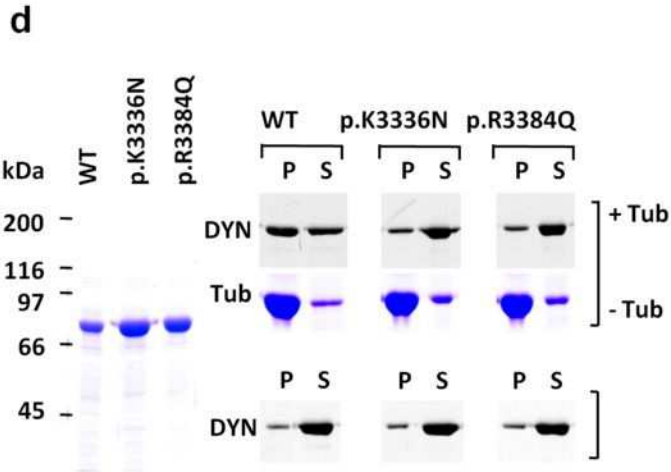
d
kDa
WT
p.K3336N
p.R3384Q
200
116
97
66
45
WT
p.K3336N
p.R3384Q
P S
P S
P S
DYN
Tub
+ Tub
- Tub
P S
P S
P S
DYN

Figure 3

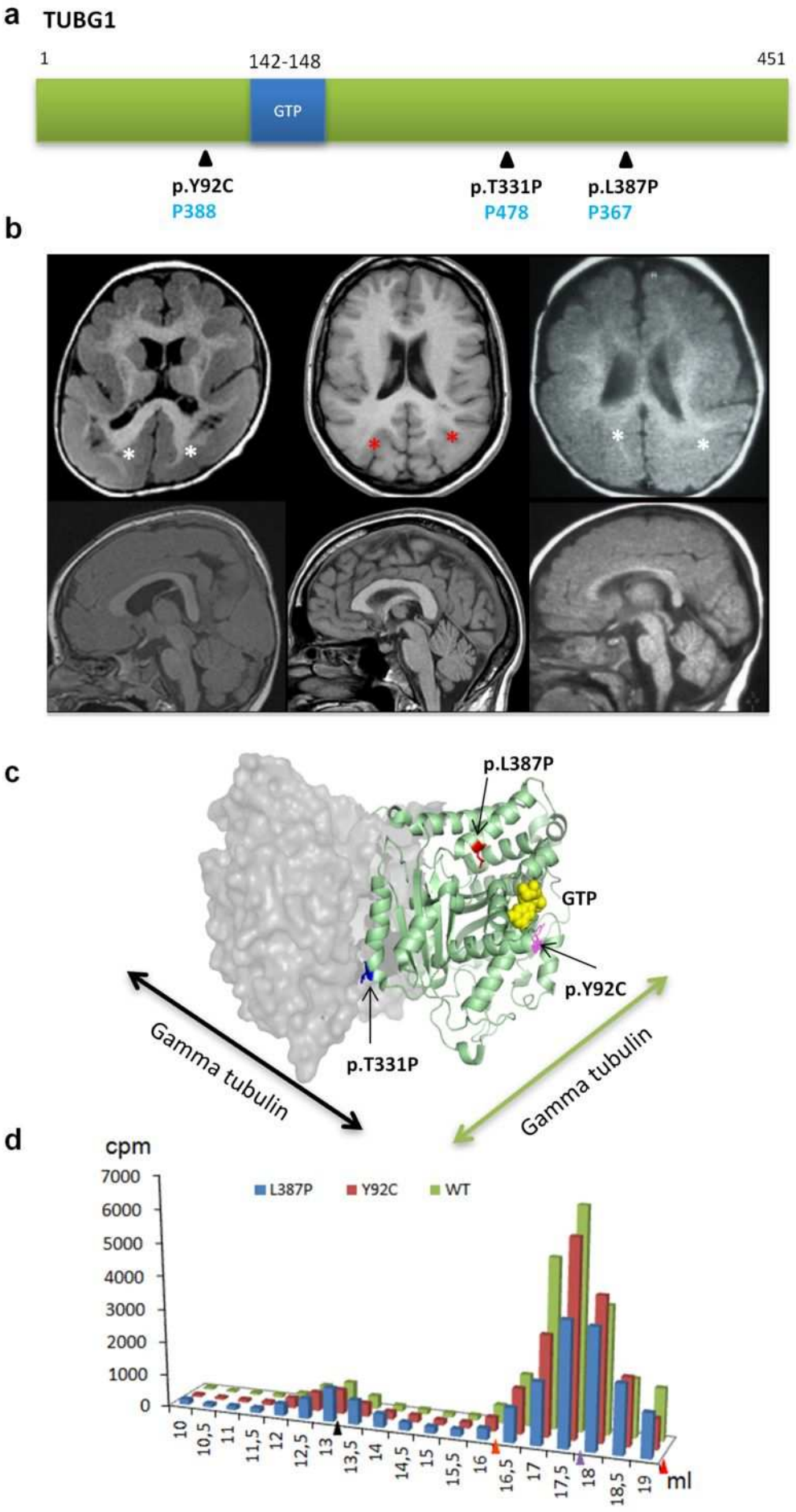
a
TUBG1
1
142-148
451
GTP
p.Y92C
P388
p.T331P
P478
p.L387P
P367
b
c
p.L387P
GTP
p.Y92C
p.T331P
Gamma tubulin
Gamma tubulin
d
cpm
7000
6000
5000
4000
3000
2000
1000
0
L387P
Y92C
WT
10
10,5
11
11,5
12
12,5
13
13,5
14
14,5
15
15,5
16
16,5
17
17,5
18
18,5
19
ml

Figure 4

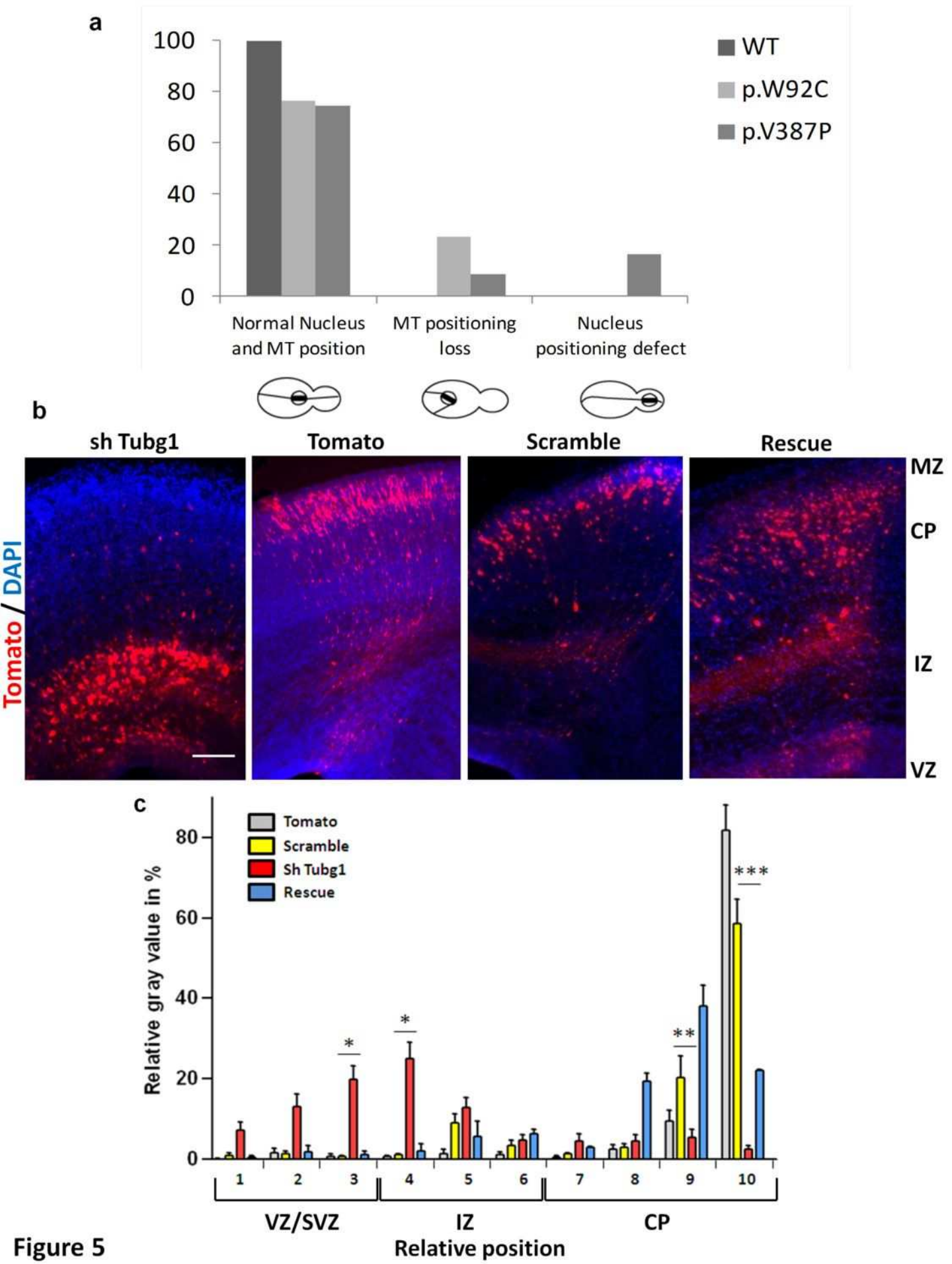
a
100
80
60
40
20
0
WT
p.W92C
p.V387P
Normal Nucleus and MT position
MT positioning loss
Nucleus positioning defect
b
sh Tubg1
Tomato
Scramble
Rescue
MZ
CP
IZ
VZ
Tomato / DAPI
c
Tomato
Scramble
Sh Tubg1
Rescue
Relative gray value in %
80
60
40
20
0
*
*
**
***
1
2
3
4
5
6
7
8
9
10
VZ/SVZ
IZ
CP
Relative position

Figure 5